Environ Earth Sci (2012) 67:1669–1677
DOI 10.1007/s12665-012-1608-0

ORIGINAL ARTICLE

Remote-sensing inversion model of surface water suspended sediment concentration based on in situ measured spectrum in Hangzhou Bay, China

Fan Wang · Bin Zhou · Xingmei Liu · Gendi Zhou · Keli Zhao

Received: 11 December 2010 / Accepted: 11 February 2012 / Published online: 24 February 2012

Abstract Suspended sediment concentration (SSC) is an important parameter for monitoring coastal water quality. Suspended particles are also the main optically active substances for ocean color remote sensing. It is important to study the surface reflectance spectra features of coastal turbid water, as it can be the basis for establishing more accurate remote-sensing inversion models. In this study, Hangzhou Bay, China, was selected as the study area. Two in situ measurement and sampling stations in the estuary of the Qiantang River which flows into Hangzhou Bay were set up separately. Above-water spectrum observation method, which the NASA recommended, was adopted to measure the reflection spectrum of turbid waters. Surface water samples were simultaneously collected to obtain the corresponding SSC data. The results showed that the total suspended particle concentrations in the Hangzhou Bay were typically high, and the inorganic suspended particle concentrations were far greater than the phytoplankton concentrations, which averages 705 mg/L and 1.16 mg/m^3. The SSC at two sampling stations both showed significant temporal variability, particularly appearing short-period rapid fluctuations accompanying the tidal cycle. The measured surface water reflectance spectra all showed typical curve characteristics of high turbid water, and as the SSC increased, the corresponding reflectivity of surface water also increased. The increments at different wavelengths were variational, with two reflectance peaks appearing at 650–700-nm and near the 800-nm wavelength of spectral curves, respectively. The first derivative of spectral curves showed that the first reflectance peak location appeared to be a "red shift" phenomenon with the SSC increasing. The correlation coefficients between the SSC of surface water and the remote-sensing reflectance according to moderate resolution imaging spectra-radiometer (MODIS) channels' central wavelength were different significantly, which were larger at MODIS long-wavelength channels (>650 nm) and smaller at MODIS short-wavelength channels (400–550 nm). The value of determination coefficient R^2 was 0.82 when the reflectance ratio of MODIS band 2 to band 1 was selected as the SSC sensitive bands combination and exponential regression analysis was employed. Therefore, the reflectance ratio of MODIS band 2 to band 1 can be adopted as the main band combination for establishing surface water SSC remote-sensing inversion model in the Hangzhou Bay.

Keywords Suspended sediment concentration · Reflectance spectral · MODIS · Remote-sensing inversion · The Hangzhou Bay

F. Wang · B. Zhou · G. Zhou (✉)
College of Life and Environmental Sciences,
Hangzhou Normal University, Hangzhou 310036, China
e-mail: zgd@zxwy.hz.gov.cn

F. Wang
e-mail: wangfan@zju.edu.cn

X. Liu (✉)
College of Environmental and Resource Sciences,
Zhejiang University, Hangzhou 310058, China
e-mail: xmliu@zju.edu.cn

K. Zhao
Zhejiang Agriculture and Forestry University,
Hangzhou 311300, China

Introduction

Using satellite remote sensing to monitor ocean surface water quality has the advantages of wide scope, high frequency, low cost and easily facilitated long-term dynamic monitoring. It

can also find the sources and migration characteristics of pollutants, which are difficult to discover by such conventional methods as field sampling. In recent years, remote sensing has gradually become a commonly used method for worldwide marine environment study, and many inversion modes have been widely developed and applied (IOCCG 2000). Not only the spectral characteristics of suspended sediments (Curran and Novo 1988), phytoplankton (Bricaud et al. 1998), yellow substance (Michael and Robert 1997), water clarity (Woodruff et al. 1999) and their remote-sensing patterns were studied, but also the experience of algorithms were established based on the statistical relationships between in situ measured concentration data and satellite remote-sensing signal (Tassan 1994).

Suspended particles in coastal waters mainly include inorganic sediments and phytoplankton, whose remote-sensing reflectance varies significantly at visible and near-infrared wavelengths according to the variation of suspended particles concentration (Curran and Novo 1988; Doxaran et al. 2006). Many oceanographers have carried out long-term research on how to obtain thematic information regarding suspended particles using water-leaving optical signals (Gordon et al. 1988). A large number of studies have focused on simulating the quantitative relationships between water-leaving radiance received by satellite and in situ measured suspended particles concentration data, and then establishing remote-sensing inversion algorithms (Curran and Novo 1988; Devred et al. 2006; Doerffer and Fischer 1994; Jerome et al. 1996). For example, the remote-sensing inversion algorithm of phytoplankton pigments concentration based on the "blue–green band ratio" has been an operational extraction algorithm and widely used in ocean color remote sensing (Bricaud et al. 1998; Carder et al. 2004; Doerffer et al. 1989; O' Reilly et al. 1998). In addition, according to the reflectance characteristic at visible and near-infrared wavelengths, the remote-sensing inversion algorithms of suspended sediment concentration (SSC) have been widely studied and applied (Curran and Novo 1988; Doerffer et al. 1989; Lavery et al. 1993; Li et al. 1998; Warrick et al. 2004). Although some research results show that the satellite remote-sensing signals of suspended sediments in turbid coastal water cannot cover up the contributions of phytoplankton (Carder et al. 2004; Doerffer et al. 1989; Lee et al. 2004), separately modeling these two kinds of suspended particles with different concentrations is feasible. However, these suspended particles have different influence mechanisms on water-leaving radiance, and not simple linear superposition (Curran and Novo 1988; Jerome et al. 1996). Therefore, in trying to build an integrated remote-sensing inversion algorithm for total suspended particles concentrations in case two water, there are still many technical and theoretical challenges (IOCCG 2000).

From the view of quantitative remote sensing, a detailed study is needed on both inherent and apparent optical properties of water to establish a more accurate remote-sensing inversion model (IOCCG 2006). To solve these problems, some scholars have established comprehensive standards of water optical measurement methods (Gordon et al. 1988; Jerome et al. 1996; Doxaran et al. 2006), which have built up a solid foundation for developing accurate remote-sensing inversions algorithms. Researches in recent years have also been carried out in China, especially about the spectral characteristics of coastal water (Wang et al. 2009). Some preliminary studies have been undertaken adopting in situ measurements. Many inversion models were estimated to simulate the relationship between remote-sensing reflectance and SSC of turbid water. (Li et al. 1998; Zhang et al. 2010). However, the optical properties of coastal waters are very complex and the compositions, such as suspended solids type, particle size distribution and concentrations, vary in different locations. At the same time, the water reflectance spectral properties are also variational in different regions around the world (Curran and Novo 1988; Tassan 1994). Accordingly, the present studies of case two water in different coastal regions are not comprehensive, especially in the coastal waters of China.

Therefore, the Hangzhou Bay, typical turbid coastal waters of China, was selected as the study area. According to NASA's ocean optical surveying criterion, we measured the water-leaving radiation spectrum and SSC of surface water. Based on the analysis of high turbid water spectral curve features and the correlation between SSC and remote-sensing reflectance of different wavelength according to the most commonly used ocean color remote-sensing satellite–MODIS channels settings, two sensitive bands were selected and an experiential remote-sensing model for SSC analysis was established. Results of this study could make up for the scarcity of in situ spectral observations in the Hangzhou Bay and could be compared with the studies for other similar high turbid coastal waters in the future.

Study area and sampling sites

The Hangzhou Bay is located approximately between 29°–32°N and 120°–123°E, in the East China Sea. In the north, it is adjacent to the estuary of the Yangtze River, which is the longest river in China (Chen et al. 2006). The western portion of the Hangzhou Bay is part of the estuary of the Qiantang River which flows across the northwest of the Zhejiang Province. As shown in Fig. 1, the shape of the Hangzhou Bay is like a trumpet with its width varying from about 21 km at the narrowest estuary to about 100 km at

Fig. 1 Study area and in situ sampling and measurement locations

the trumpet mouth. The average depth of the Hangzhou Bay is about 10 m and the total water area is about 5,000 km^2. The seabed of the Hangzhou Bay is a both undulating and contractive plane, and tidal range increases rapidly from east to west, with tidal peaks appearing at the estuary of the Qiantang River. Under the common influences of the Yangtze River estuary south flowing water, the Qiantang River runoff and the East China Sea tidal waves, this study area has typical coastal waters characteristics, which include strong tides, rapid flow and high concentrations of suspended sediments (Gao et al. 1993; Su and Wang 1989).

The inherent optical properties of coastal water have the characteristics of spatial and temporal variability, which is the reason for developing site-specific remote-sensing inversion algorithms for different coastal water (IOCCG 2000; Jerome et al. 1996). In order to quantify the relationship between remote-sensing reflectance and SSC of surface water, in situ spectral measurement and water samples collection should be continuous and simultaneous (Curran and Novo 1988; IOCCG 2006). In September 2007, surface water samples were obtained from two sampling stations—Zhapu and Cixi—which are in the north and south of the Hangzhou Bay estuary, separately. The study area and field sampling positions are shown in Fig. 1. At each field station, the samples were collected from 9:00 a.m. to 4:00 p.m. at intervals of half hour continuously within a day. The water spectrums were measured and the samples of surface water were synchronously collected to obtain a tidal-cycle time series data set. The total in situ data set of 35 samples was prepared for further statistical analysis.

Materials and methods

Spectral observation geometry

In this study, the spectrums of turbid water were measured by in situ above-water observation method using a portable

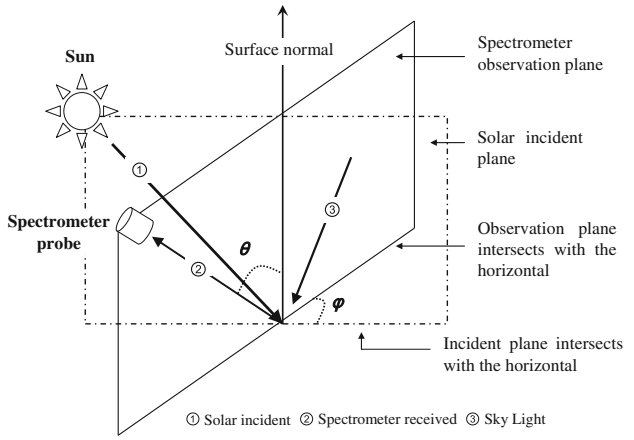

Fig. 2 Viewing geometry of above-water measurement (Mobley 1999)

ASD spectroradiometer and 30% reflectance standard plate. The radiances of water, sky scattered light and standard plate were measured, and then the water-leaving radiation and remote-sensing reflectance were calculated. To avoid direct sunlight reflection, the shadow of the ship and other carriers influencing the water surface light field, there are two typical observation geometry settings in international water color study at present, (1) $\varphi = 90°$, $\theta = 20°$; (2) $\varphi = 135°$, $\theta = 40°$, where φ is the angle between solar incident plane and spectrometer observation plane, and θ is the angle between the water surface normal and the spectrometer observation direction (Mobley 1999; Mueller et al. 2003). Both methods have their advantages and disadvantages and there is still no uniform opinion by researchers regarding how to set the observation geometry. The Sensor Intercomparison for Marine Biological and Interdisciplinary Ocean Studies (SIMBIOS) program recommends the second observation geometry and the NASA ocean optical observation standards also recommend taking advantage of (40°, 135°) as the observation angle (Mueller et al. 2003). In this study, the observations geometry of spectrometer adopt NASA specifications recommended (40°, 135°) viewing angle setting, in which the angle between the instrument observation plane and sun incidence plane is 135° (back to sun direction), and the angle between the equipment observation direction and water surface normal is 40°. Each successive continuous measurement time should at least overpass a wave period, and so the instrument integration time was fixed as 136 ms. Spectral observation geometry settings are according to Fig. 2.

Remote-sensing reflectance

In order to establish the quantitative relationships between the in situ spectral measurement data and satellite remote sensing, the field measurement data are processed to obtain water-leaving radiance and remote-sensing reflectance based on the water, sky and standards board radiance (Doxaran et al. 2006; Jerome et al. 1996). When avoiding direct sunlight in the reflection, ignoring the impact of surface foam from the external circumstances and fixing the integration time for the spectrometer, the remote-sensing reflectance of water surface can be calculated according to formula (1):

$$R_{\mathrm{rs}} = \frac{\left(L_{\mathrm{w}} - \rho L_{\mathrm{sky}}\right)\rho_{\mathrm{p}}}{\pi E_{\mathrm{s}}} \quad (1)$$

In the formula, L_{w}, L_{sky} and E_{s}, respectively, are the spectrometer measurements value of water, sky and the standard plate, and ρ_{p} is the reflectivity of strict calibration standards plate. ρ is the reflectivity of air–water interface to the sky light, depending on the position of the sun, the radiation distribution of sky light, spectrometer observation geometry, wind speed and wind direction or surface roughness and other factors, whose value usually is between 0.02 and 0.06 (Mueller et al. 2003). According to Mobley's study, in sunny, low wind speed and 40° observation angle, ρ value can be 0.028 (Mobley 1999).

Suspended particles concentration

Surface water samples were collected at the same time of the spectral measurements according to NASA ocean optical observation standards, stored in cold and black boxes, and brought back to measure their concentrations in laboratory. Water samples mainly include two kinds of suspended solids, which are inorganic (suspended sediments) and organic (phytoplankton) materials. The concentration of phytoplankton usually can be indicated by the chlorophyll-*a* (O' Reilly et al. 1998; Devred et al. 2006). Suspended sediment concentrations were measured by a "weight method" and the chlorophyll concentration was measured by spectrophotometer (Li et al. 1998; O' Reilly et al. 1998). First, water samples were treated by vacuum filtration, after membrane extraction with acetone, and then centrifuged. Finally, the absorbance of the supernatants, which were placed on the spectrophotometer, using 1 cm optical path cuvette, were measured at 750, 664, 647 and 630-nm wavelength, and then the concentration of chlorophyll was calculated according to formula (2):

$$C_{\mathrm{chl-a}} = (11.85E_{664} - 1.54E_{647} - 0.08E_{630}) \times \frac{v}{V \times l} \quad (2)$$

In this formula, E_{664}, E_{647} and E_{630}, respectively, are the adjusted absorbance values of 664, 647 and 630-nm wavelengths minus absorbance at 750 nm, v is the extract supernatant volume (mL) of each sample, V is water sample volume (L), and l is the cuvette optical path length

(cm). The water samples were filtered using 0.45-μm pore size cellulose acetate and glass fiber filter membrane.

Results and discussion

Temporal and spatial variability of suspended particles concentrations

Measurement results showed that the total concentrations of suspended particles in surface water of the Hangzhou Bay were high and appeared to have significant spatial and temporal variability characteristics. Firstly, the SSC with an average of 705 mg/L was greater than chlorophyll concentrations, which averaged 1.164 mg/m^3 (Table 1). Secondly, the average SSC at Zhapu station was less than SSC at the Cixi station, which was mainly due to the underwater topography of the two stations. There are deep grooves at the Zhapu station, while the Cixi station underwater has a shallow shoal (Wang and Eisma 1990). Finally, the SSC of these two stations also showed significant variation at short time scales (Fig. 3), which may be due to the influence of the south-flowing turbid water of the Yangtze River estuary and the bottom sediment re-suspension under tide lifting action (Chen et al. 2006). The variation of short time scales showed that in situ ground measurements and satellite received data should be synchronized when establishing the remote-sensing inversion experience algorithms of SSC in high tide energy coastal areas similar to the Hangzhou Bay. Otherwise, it would be difficult to obtain accurate statistical correlations.

Water surface reflectance spectral characteristics

Above-water spectrum measurement is continuous at each station, at half-hour intervals accompanied with surface water sampling. Results showed that the water surface reflectivity of the Hangzhou Bay were dominated by suspended sediments and the reflectance spectra showed typical curve characteristics of high turbid water as in other studies of the coastal area (Curran and Novo 1988; Doerffer et al. 1989; Doxaran et al. 2006; Zhang et al. 2010). Figure 4a, b, presents the measured reflectivity spectrum and their first derivative curves at different sampling times within 1 day. As shown in Fig. 4a, the water surface reflectance changed with the wavelength. There were two reflection peaks in the visible band: the first appeared between 650 and 700 nm, and the other was around 800 nm. The reflection valley appeared around 750 nm. When SSC is low, the first reflection peak is higher than the second reflection peak. With SSC increasing, the increment of water reflectivity varied between the two reflection peaks. The reflectivity increasing rate at the second peak was higher than that at the first one, and the "shoulder" of both sides of the second reflection peak also increased rapidly.

Estimating spectral curves by a first derivative treatment can eliminate the influence of some linear change factors in the measurement environment, which helps to obtain an objective analysis of spectral curve shape changes (Mueller et al. 2003). The positive or negative value of the first derivative reflectance spectra curve, respectively, indicates the up or down trend of water reflectivity. The maximum and minimum value can represent the most prominent changing position of the spectral curve, while the value of zero represents the reflection peak or valley of the reflectance spectrum curve. As shown in Fig. 4b, the shapes of the first derivative spectral curves for different SSC are basically similar, with some significant differences in several wavelengths. First, the emergence places of the first zero value for

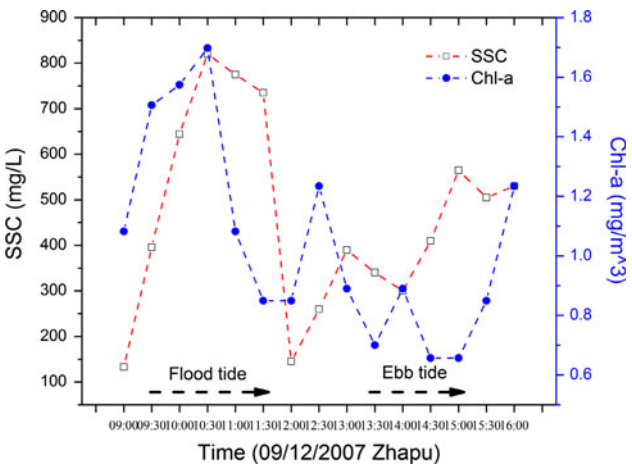

Fig. 3 Temporal variations of suspended particles concentrations in relation to tide flood and ebb at Zhapu sampling site. The *arrows* indicate different tidal situations

Table 1 Statistical characteristics of measured suspended particles concentrations at different sample sites

Sample site	Suspended particle	Maximum	Minimum	Mean	Samples number
Zha Pu	Suspended sediment (mg L^{-1})	820	133	463	35
	Phytoplankton chlorophyll (mg m^{-3})	1.69	0.66	1.05	35
Ci Xi	Suspended sediment (mg L^{-1})	1,950	700	1,224	35
	Phytoplankton chlorophyll (mg m^{-3})	2.31	1.74	2.03	35

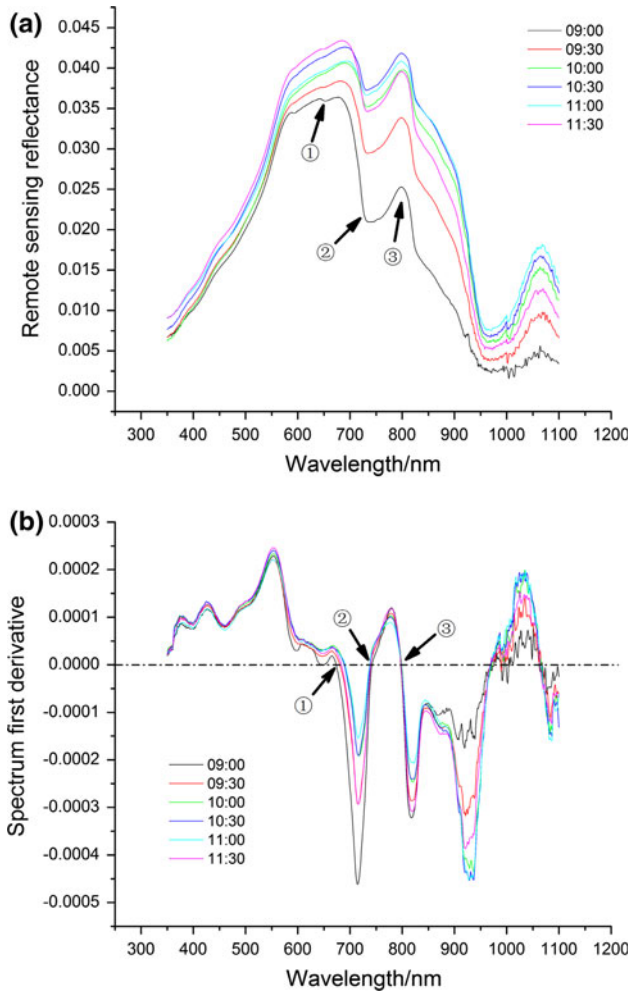

Fig. 4 Above-water remote-sensing reflectance spectrum and their first derivative curves according to SSC variation from 9:00 to 11:30 on 09/12/2007 at the Zhapu station. The *arrows* indicate the reflectance peak and valley, in which *arrow*① aim at the first reflectance peak, *arrow*② point to the reflectance valley, and *arrow*③ present the second reflectance peak. The *arrow*① of (**b**) shows the apparent "*red* shift" phenomenon of the first reflectance peak

different curves gradually moved to longer wavelengths, corresponding to that of the first reflection peak of the spectral curve shift to longer wavelength, which is the so-called "red shift" phenomenon (Curran and Novo 1988). Secondly, the reflection valley and the second reflection peak at the zero positions were basically with the same wavelength, which appeared as a "saturation" phenomenon. It showed that with rising SSC, the reflectance ratio of red–green band became saturated, which means that the water surface reflectivity is insensitive to the change of water SSC.

Correlations between remote-sensing reflectance and SSC

Water surface remote-sensing reflectance at different wavelengths has various responses to SSC changes. When choosing sensitive bands for the turbid water and fitting the statistical relationships between SSC and remote-sensing reflectance (R_{rs}), the SSC information of surface water can be obtained by remote-sensing inversion (Doerffer et al. 1989; Li et al. 1998; Miller and Brent 2004; Zhang et al. 2010). In this study, according to MODIS visible and near-infrared channel settings (Table 2), the statistical relationships between remote-sensing reflectance at different MODIS channels and SSC were analyzed, and then the bands sensitive to SSC variety were appraised. Figure 5 shows the correlation coefficient curves. The correlation coefficients between water remote-sensing reflectance and SSC are relatively low in MODIS short-wavelength channel whose central wavelengths are at 400–550 nm, and less than 0.5. But when MODIS center wavelength channels are longer than 650 nm, the correlation coefficients are more than 0.5. Especially at the MODIS near-infrared channels, the correlation coefficients are more than 0.8. These results indicated that the range of visible and near-infrared wavelengths is suitable for monitoring the surface water SSC. Especially, the wavelength channels at 700–900 nm are sensitive to the variety of SSC in high turbid coastal water. These results are similar to those in other studies on SSC remote-sensing inversion (Doerffer et al. 1989; Li et al. 1998; Miller and Brent 2004; Pattiaratchi et al. 1994; Zhang et al. 2010).

In addition, as shown in Fig. 5, the correlation coefficient between the natural logarithm of SSC (LnSSC) and MODIS bands reflectance did not increase significantly, when compared with the non-log transformation. Also, for some bands, the correlation coefficient even got lower. Therefore, when establishing the statistical regression model in this study, we used the SSC data without log transformation.

Table 2 Features of MODIS channels

Channel name	Spectral range (nm)	Central wavelength (nm)	SNR	Spatial resolution (m)
1	620–670	645	128	250
2	841–876	858	201	250
3	459–479	469	243	500
4	545–565	555	228	500
8	405–420	412	880	1,000
9	438–448	443	838	1,000
10	483–493	488	802	1,000
11	526–536	531	754	1,000
12	546–556	551	750	1,000
13	662–672	667	910	1,000
14	673–683	678	1,087	1,000
15	743–753	748	586	1,000

SNR ratio of signal and noise

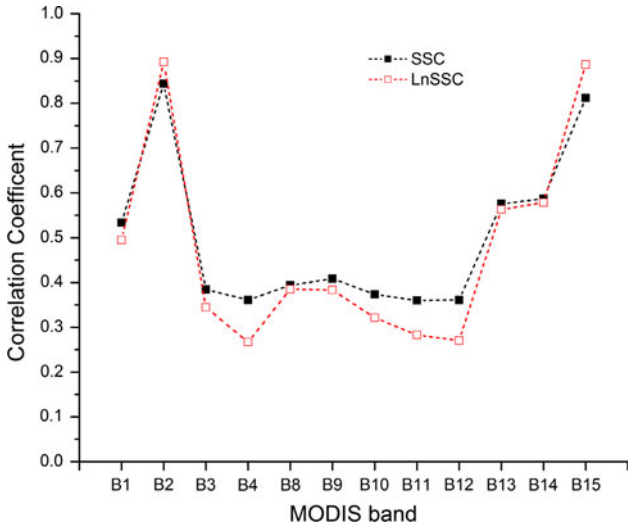

Fig. 5 Correlation coefficients between SSC and remote-sensing reflectance at different MODIS band central wavelengths. B_i ($i = 1, 2, 3,\ldots,15$) indicate different MODIS bands central wavelengths. LnSSC represents the natural logarithm of SSC

MODIS bands sensitive to SSC

The water-leaving radiances are determined by absorption and backscatter of water molecules, suspended material and soluble yellow substances (Gordon et al. 1988). Only if the absorption of water itself, yellow substance and algal chlorophyll is very small can we get more information on the true concentration of suspended sediments. The strong absorption of water itself is at near-infrared wavelength (Pope and Fry 1997); the soluble yellow substances absorb the shorter wavelength radiation strongly, while the radiation absorption of the shorter than 600-nm band is almost 0 (Doerffer and Fischer 1994). Additionally, many studies showed that the main influence of pigment absorption on water reflectance spectra concentrates happened between the 400 and 700-nm wavelengths, which usually appear as two absorption peaks at the 425 and 675-nm wavelengths (Bricaud et al. 1998; Carder et al. 2004). Therefore, to induce the absorption influence of water, soluble yellow substances and algal chlorophyll, absorption wavelength ranges should be avoided.

The wavelength range of ASD spectrometer used in this study is between 380 and 1050 nm, so the sensitive bands should be selected only at the intersection of MODIS channels setting and spectrometer wavelength range, where there are mainly the MODIS visible and near-infrared bands. In addition, when selecting MODIS bands which are sensitive to SSC remote-sensing inversion of coastal water, the spatial resolution and the ratio of signal and noise (SNR) should be evaluated. The selection method is based on the correlation coefficients between water SSC and the remote-sensing reflectance. As shown in Figs. 4, 5, the center wavelengths of MODIS 1 and 2 channels are in the vicinity of the two reflection peaks of spectral curves, and the correlation coefficients between their remote-sensing reflectance and SSC are 0.53 and 0.84, respectively. Moreover, their 250-m spatial resolution and lower SNR are appropriate for water color remote sensing in narrow estuaries and coastal waters. Although there is better correlation coefficient between water SSC and MODIS band 15 remote-sensing reflectance, whose central wavelength is 748 nm, the spatial resolution and SNR of MODIS band 15 are unsuited for this study area.

Statistical regression models

While comprehensively considering the correlation coefficient, spatial resolution and SNR, MODIS band 1 and band 2 were chosen as the basic bands for establishing SSC remote-sensing inversion models. Referring to some similar studies (Curran and Novo 1988; Miller and Brent 2004), these two bands were composed or transformed, and simple linear regression, exponential regression and power function regression were analyzed. The band transforming methods and fitting equations are shown as follows:

$$R_1 = R_{\mathrm{rs}}(\mathrm{Band1}) \tag{3}$$

$$R_2 = R_{\mathrm{rs}}(\mathrm{Band2}) \tag{4}$$

$$R_3 = R_{\mathrm{rs}}(\mathrm{Band1})/R_{\mathrm{rs}}(\mathrm{Band2}) \tag{5}$$

$$R_4 = (R_{\mathrm{rs}}(\mathrm{Band1}) + R_{\mathrm{rs}}(\mathrm{Band2}))/(R_{\mathrm{rs}}(\mathrm{Band1})/R_{\mathrm{rs}}(\mathrm{Band2})) \tag{6}$$

$$S = a \cdot R_i + b \tag{7}$$

$$S = a \cdot e^{b \cdot R_i} \tag{8}$$

$$S = a \cdot R_i^b. \tag{9}$$

In these formulae, R_i ($i = 1, 2, 3, 4$) are the values of MODIS band remote-sensing reflectance and its transformation, S is the SSC, and a and b are regression coefficients. The statistical regression results showed that the simple linear regression between the remote-sensing reflectance of MODIS band 2 and SSC was best, and the

Table 3 Results of linear regression between SSC and MODIS bands' remote-sensing reflectance, in which R^2 is determinant coefficient, and A and B are the regression parameters

Linear regression parameters	R_1	R_2	R_3	R_4
R^2	0.29	0.71	0.64	0.32
A	83.89	49.31	2.12	−12.33
B	−2.72	−0.66	−0.76	1.88

R_i ($i = 1, 2, 3, 4$) are the remote-sensing reflectance of MODIS band 1 and band 2, and their combined transformations

coefficient of determination (R^2) was 0.71 (Table 3). Figure 6 shows other statistical regression results based on the least square method between the reflectance transformations of MODIS bands and SSC. The determination coefficients of these regression equations are representative of the goodness of fit. They indicated that both power function regression and exponential regression achieved better fitting results when the ratio of MODIS band 2 reflectance and band 1 reflectance were adopted. Their coefficients of determination were all above 0.8. As shown in Fig. 6, the best R^2 was 0.82 when both the reflectance ratio of MODIS band 2 to band 1 and exponential regression method were adopted.

Conclusion

Based on in situ above-water spectrum measurement and surface water sampling in the Hangzhou Bay, the relationships between remote-sensing reflectance and SSC of surface water were appraised. Measurement results showed that the total concentrations of suspended particles of surface water were high and appeared to have significant spatial and temporal variability characteristics at two sampling stations. The surface water reflectance spectra showed typical curve characteristics of highly turbid water, indicating that suspended sediments dominated the reflectance spectral curve of surface water in this study area. The water spectral analysis results indicated that there appeared a "red shift" phenomenon accompanying SSC increase at the first reflectance peak location. The correlation coefficients between water SSC and remote-sensing reflectance varied at different wavelengths.

Atmosphere affects the solar radiation weakly at the atmospheric window within the range of visible and near-infrared wavelength. For the visible and near-infrared bands, the strong atmosphere water vapor absorption bands are at 0.71–0.735, 0.81–0.84 and 0.89–0.99 μm. The MODIS band 1 of 620–670 nm and MODIS band 2 of 841–876 nm can avoid the strong atmosphere water vapor absorption. Other satellites, such as Landset TM 4 with the wavelength range of 0.76–0.90 μm and SPOT multispectral channel three with wavelength range of 0.78–0.89 μm also take into consideration the effect of atmosphere window. Synthetically considering spatial resolution and the ratio of signal to noise of MODIS channels, MODIS 1 and band 2 were selected as sensitive channels for establishing SSC remote-sensing inversion models in this study. Different regression analysis results indicated that experiential models could achieve good coefficients of determination. The best R^2 was 0.82 when the remote-sensing reflectance ratio of MODIS band 2 to band 1 was adopted as regression variable, and an exponential regression method was employed. When validated by satellite remote-sensing images, this band combination and regression analysis method can be practically operated as surface water SSC

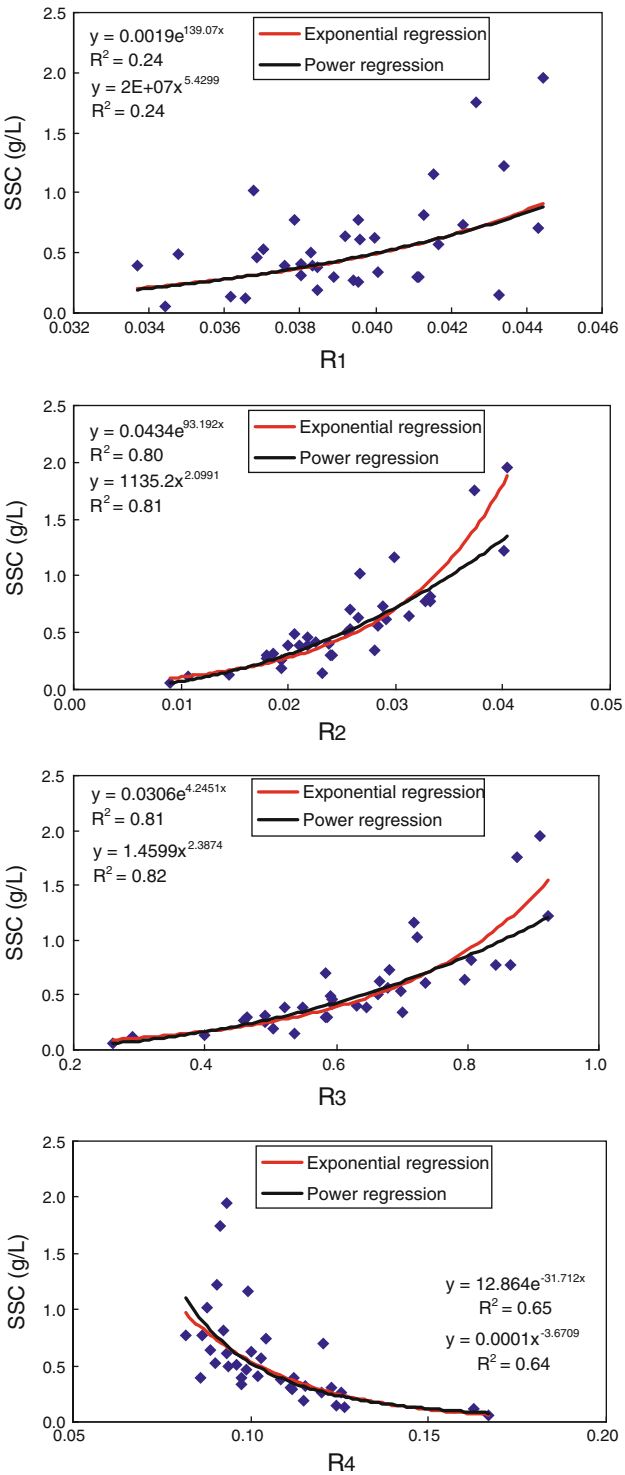

Fig. 6 Results and curves of different regression models including exponential regression and power regression, in which R^2 is determinant coefficient. R_i ($i = 1, 2, 3, 4$) are remote-sensing reflectance of MODIS band 1 and band 2, and their combined transformations

remote-sensing inversion model in the Hangzhou Bay. As is well known, the inherent optical characteristics for coastal waters are complex and varied. The remote-sensing inversion model based on experiential algorithms has its limit and is not suitable for all case two waters. However, the methods by which the models were developed in this study could provide valuable information for other studies on similar turbid coastal waters. In order to develop a high-precision remote-sensing inversion model for coastal waters, the analytical algorithms have to be built based on the relationships among water parameter concentrations, inherent optical character and apparent optical parameters.

Acknowledgments This research was sponsored by the National Natural Science Foundation of China (40901254, 40971193) and the Project of Zhejiang Key Scientific and Technological Innovation Team (2010R50039). The authors would like to thank the Institute of Hydraulics and Estuary of Zhejiang Province for providing much useful tide information about the study area. The authors also thank Professor Earl Bossard from San Jose State University for providing precious suggestions and English presentation revisions. We also wish to thank the anonymous reviewers and editor-in-chief for reviewing the paper.

References

Bricaud A, Morel A, Babin M, Allali K, Claustre H (1998) Variations of light absorption by suspended particles with chlorophyll *a* concentration in oceanic (case 1) waters: analysis and implications for bio-optical models. J Geophys Res 103:31033–31044

Carder KL, Chen FR, Cannizzaro JP, Campbell JW (2004) Performance of the MODIS semi-analytical ocean color algorithm for chlorophyll-*a*. Adv Space Res 33(7):1152–1159

Chen SL, Zhang GA, Yang SL, John ZS (2006) Temporal variations of fine suspended sediment concentration in the Changjiang River estuary and adjacent coastal waters, China. J Hydrol 133:137–145

Curran PJ, Novo EMM (1988) The relationship between suspended sediment concentration and remotely sensed spectral radiance: a review. J Coast Res 4:351–368

Devred E, Sathyendranath S, Stuart V, Maass H, Ulloa O, Platt T (2006) A two component model of phytoplankton absorption in the open ocean: theory and applications. J Geophys Res 111:C03011

Doerffer R, Fischer J (1994) Concentrations of chlorophyll, suspended matter, and gelbstoff in case 2 waters derived from satellite coastal zone color scanner data with inverse modeling methods. J Geophys Res 99:7457–7466

Doerffer R, Fischer J, Stossel M, Brockmann C (1989) Analysis of Thematic Mapper data for studying the suspended matter distribution in the coastal area of the Germany Bight (North Sea). Remote Sens Environ 28:61–73

Doxaran D, Cherukuru N, Lavender SJ (2006) Apparent and inherent optical properties of turbid estuarine waters: measurements, empirical quantification relationships, and modeling. Appl Opt 45(10):2310–2324

Gao SQ, Yu GH, Wang YH (1993) Distributional features and fluxes of dissolved nitrogen, phosphorus and silicon in the Hangzhou Bay. Mar Chem 43:65–81

Gordon HR, Brown OB, Evans RH et al (1988) A semianalytic radiance model of ocean color. J Geophys Res 93:10909–10924

IOCCG (2000). Remote sensing of ocean color in coastal and other optically complex waters, vol 3 International Ocean-Color Coordinating Group, Dartmouth, CanadaTech. Report

IOCCG (2006). Remote sensing of inherent optical properties: fundamentals, tests of algorithms, and applications, vol 5 International Ocean-Color Coordinating Group, Dartmouth, CanadaTech. Report

Jerome J, Bukata R, Miller J (1996) Remote sensing reflectance and its relationship to optical properties of natural waters. Int J Remote Sens 17:3135–3155

Lavery P, Pattiaratchi C, Wyllie A, Hick P (1993) Water quality monitoring in estuarine water using the Landsat Thematic Mapper. Remote Sens Environ 46:268–280

Lee ZP, Carder KL, Du KP (2004) Effects of molecular and particle scatterings on model parameters for remote-sensing reflectance. Appl Opt 43:4957–4964

Li Y, Wei H, Ming F (1998) An algorithm for the retrieval of suspended sediment in coastal waters of China from AVHRR data. Cont Shelf Res 18:487–500

Michael S, Robert AA (1997) Effect of suspended particulate and dissolved organic matter on remote sensing of coastal and riverine waters. Appl Opt 27:6905–6912

Miller RL, Brent AM (2004) Using MODIS Terra 250 m imagery to map concentrations of total suspended matter in coastal waters. Remote Sens Environ 93:259–266

Mobley CD (1999) Estimation of the remote-sensing reflectance from above-surface measurements. Appl Opt 38:7442–7455

Mueller JL et al (2003) Ocean optics protocols for satellite ocean color sensor validation, revision 4, vol 3: Radiometric measurements and data analysis protocols, NASA/TM-2003-211621

O' Reilly J, Maritorena S, Mitchell BG, Siegel D, Carder KL, Garver S et al (1998) Ocean color chlorophyll algorithms for SeaWiFS. J Geophys Res 103:24937–24953

Pattiaratchi C, Lavery P, Wyllie A, Hick P (1994) Estimates of water quality in coastal waters using multi date Landsat Thematic Mapper data. Int J Remote Sens 15:1571–1584

Pope RM, Fry ES (1997) Absorption spectrum (380–700 nm) of pure water.2. Integrating cavity measurements. Appl Opt 36(33): 8710–8723

Su JL, Wang KS (1989) Changjiang River Plume and suspended sediment transport in Hangzhou Bay. Cont Shelf Res 9:93–111

Tassan S (1994) Local algorithms using SeaWiFS data for the retrieval of phytoplankton, pigments, suspended sediment, and yellow substance in coastal waters. Appl Opt 33(12):2369–2378

Wang BC, Eisma D (1990) Supply and deposition of sediment along the north bank of Hangzhou Bay China. Neth J Sea Res 25(3): 377–390

Wang F, Zhou B, Xu JM (2009) Application of neural network and MODIS 250 m imagery for estimating suspended sediments concentration in Hangzhou Bay, China. Environ Geol 56: 1093–1101

Warrick JA, Mertes KA, Siegel DA, Mackenzie C (2004) Estimating suspended sediment concentrations in turbid coastal waters of the Santa Barbara Channel with SeaWiFS. Int J Remote Sens 25(10):1995–2002

Woodruff DL, Stumpf RP, Scope JA, Paerl HW (1999) Remote estimation of water clarity in optically complex estuarine waters. Remote Sens Environ 68:41–52

Zhang MW, Tang JW, Dong Q, Song QT, Ding J (2010) Retrieval of total suspended matter concentration in the Yellow and East China Seas from MODIS imagery. Remote Sens Environ 114: 392–403